

# Gas Phase Reaction Kinetics of O Atoms with (CH<sub>3</sub>)<sub>2</sub>NNH<sub>2</sub>, CH<sub>3</sub>NHNH<sub>2</sub>, and N<sub>2</sub>H<sub>4</sub>, and Branching Ratios of the OH Product

Ghanshyam L. Vaghjiani<sup>†</sup>

ERC, Inc. Air Force Research Laboratory, AFRL/PRSA, 10 East Saturn Boulevard,  
Edwards Air Force Base, California 93524

Received: December 14, 2000; In Final Form: March 6, 2001

The gas-phase reaction kinetics of O atoms with the two alkylated diamine rocket fuels, (CH<sub>3</sub>)<sub>2</sub>NNH<sub>2</sub> and CH<sub>3</sub>NHNH<sub>2</sub>, was studied in a discharge flow-tube apparatus under pseudo-first-order conditions in [O atom]. Direct vuv cw-resonance fluorescence monitoring of the [O atom] temporal profiles in a known excess of the [diamine] yielded the following absolute second-order O atom rate coefficient expressions:  $k_1 = (1.94 \pm 0.34) \times 10^{-11} e^{(25 \pm 25)/T}$  and  $k_2 = (2.29 \pm 0.40) \times 10^{-11} e^{(-145 \pm 40)/T}$  cm<sup>3</sup> molecule<sup>-1</sup> s<sup>-1</sup>, respectively, for reactions with (CH<sub>3</sub>)<sub>2</sub>NNH<sub>2</sub> and CH<sub>3</sub>NHNH<sub>2</sub> in the temperature range 232–644 K and in He pressure of 2.0 Torr. The total yields of OH in the reactions were measured to be (0.12 ± 0.09) and (0.14 ± 0.10) at 298 K and in 2.0 Torr He pressure. Close to ~ 53% and ~ 59% of the OH produced was estimated to be vibrationally excited. A pulsed-photolysis reactor was used to extend our measurements on the O atom reaction kinetics with the unsubstituted rocket fuel, N<sub>2</sub>H<sub>4</sub> that we had previously studied in the flow-tube apparatus. At 298 K, both the rate coefficient,  $k_3 = (0.59 \pm 0.12) \times 10^{-11}$  cm<sup>3</sup> molecule<sup>-1</sup> s<sup>-1</sup> and the total OH yield = (0.35 ± 0.14) did not show any discernible dependence on He or N<sub>2</sub> buffer gas pressures of up to 404 Torr. The magnitude of, the weak temperature dependence and the lack of pressure effect in the O + N<sub>2</sub>H<sub>4</sub> reaction rate coefficient suggests that simple direct metathesis of H atom may not be important compared to initial addition of the O atom to the diamine, followed by rapid dissociation of the intermediate into a variety of products.

## Introduction

Hydrazine (N<sub>2</sub>H<sub>4</sub>), methylhydrazine (CH<sub>3</sub>NHNH<sub>2</sub>) and unsymmetrical dimethylhydrazine ((CH<sub>3</sub>)<sub>2</sub>NNH<sub>2</sub>) form an important class of diamine based rocket fuels.<sup>1</sup> They are typically oxidized in nitrogen tetroxide (N<sub>2</sub>O<sub>4</sub>) combustors to generate the desired thrust. For example, a blend of 50:50 N<sub>2</sub>H<sub>4</sub> and (CH<sub>3</sub>)<sub>2</sub>NNH<sub>2</sub> is deployed in the Titan launch vehicles and CH<sub>3</sub>NHNH<sub>2</sub> is used in the various Space Shuttle thrusters that make up the orbital maneuver system (OMS) and the reaction control system (RCS). Their use as monopropellants, especially that of N<sub>2</sub>H<sub>4</sub>, is also very common in small attitude and trajectory control systems of many satellites. Rocket exhaust effluents, which can include raw fuel fragments, are known not only to reduce the lifetime or the performance of the onboard instrumentation due to surface contamination,<sup>2</sup> but also to degrade the ambient atmospheric optical environment due to chemiluminescent interactions both in the near and far-fields of the expanding plume. Emissions ranging from the IR to the vuv are possible that primarily arise due to on going combustion reactions in the near-field (core radiation)<sup>3</sup> and due to effluent-atmosphere collisions in the far-field (plume radiation).<sup>4–8</sup> The most recent ground-based<sup>9</sup> and in-flight<sup>4,10</sup> observations of the UV-visible emissions from the Space Shuttle's thrusters have reported intense 336 nm NH(A→X) and 630 nm O(<sup>1</sup>D→<sup>3</sup>P), and strong 558 nm O(<sup>1</sup>S→<sup>1</sup>D) features in the plume radiation. Analysis and modeling of these features as a function of ram-angle and altitude indicate that the mechanism for O(<sup>1</sup>S)/O(<sup>1</sup>D) production is via collisional excitation of atmospheric O(<sup>3</sup>P) by the exhaust effluents, H<sub>2</sub>O and/or N<sub>2</sub>, and for NH(A) production

via the O(<sup>3</sup>P) + CH<sub>2</sub>NH reaction. The CH<sub>2</sub>NH fragment is believed to come from the thermal decomposition of the escaping fuel, CH<sub>3</sub>NHNH<sub>2</sub>. Clear explanations of the source(s) for many other weaker emission features (OH(A→X), NO(A→X), CN(B→X), CO(a→X), etc.) in Space Shuttle plume radiation have not yet been proposed. This must wait until we have a detailed understanding of the processes that control the temporal and spatial evolution of the initial exhaust effluents and their subsequent products. The three main processes that determine the fate of the diamine fuel fragments within the thermospheric plume are degradation by pyrolysis, oxidation by O atoms, and heterogeneous loss to spacecraft surfaces. It is therefore desirable to accurately determine the product distributions and the reactivity trends in O atom reactions with diamines not only for carrying out reliable plume-radiance calculations but also for properly simulating the combustion of these fuels in N<sub>2</sub>O<sub>4</sub>.

There is only one previous report<sup>11</sup> on the room temperature (296 K) values for the O atom rate coefficients:  $k_1 = (2.3 \pm 0.34) \times 10^{-11}$  and  $k_2 = (1.6 \pm 0.34) \times 10^{-11}$  cm<sup>3</sup> molecule<sup>-1</sup> s<sup>-1</sup>, respectively, for reaction with (CH<sub>3</sub>)<sub>2</sub>NNH<sub>2</sub> and CH<sub>3</sub>NHNH<sub>2</sub>. In the same study  $k_3 = (0.99 \pm 0.12) \times 10^{-11}$  cm<sup>3</sup> molecule<sup>-1</sup> s<sup>-1</sup> for the O + N<sub>2</sub>H<sub>4</sub> reaction was also reported. Two other room-temperature values for  $k_3 = (0.30 \pm 0.15) \times 10^{-11}$  and  $= 1.82 \times 10^{-11}$  cm<sup>3</sup> molecule<sup>-1</sup> s<sup>-1</sup> can also be found in the literature.<sup>12,13</sup> All these values differ significantly from our previous value of  $(0.61 \pm 0.11) \times 10^{-11}$  cm<sup>3</sup> molecule<sup>-1</sup> s<sup>-1</sup> measured in a flow-tube apparatus.<sup>14</sup> Furthermore, we measured a negative temperature dependence for  $k_3 = (7.35 \pm 2.16) \times 10^{-13} \exp[(640 \pm 60)/T]$ , in the temperature range 252–423 K and in 2.0 Torr He pressure, whereas a positive dependence of  $1.4 \times 10^{-10} \exp[-604/T]$  cm<sup>3</sup> molecule<sup>-1</sup> s<sup>-1</sup> in

<sup>†</sup> Phone: 661-275-5657. Fax: 661-275-6245. Email: ghanshyam.vaghjiani@edwards.af.mil.

the temperature range 243–463 K and in 1–10 Torr of Ar pressure had been claimed in ref 13. Accurate product yield measurements in the above three reactions are also scarce. For O + N<sub>2</sub>H<sub>4</sub> reaction, an OH yield of (0.15 ± 0.05) at 298 K and in 2.0 Torr of He pressure was previously reported by us.<sup>14</sup> This low yield is consistent with Foner and Hudson's<sup>15</sup> mass spectrometric observations of N<sub>2</sub>H<sub>3</sub> product intensity being ~25 times smaller than that of the N<sub>2</sub>H<sub>2</sub> product in their crossed molecular beam investigations of the O + N<sub>2</sub>H<sub>4</sub> interaction. Similarly, in the O + (CH<sub>3</sub>)<sub>2</sub>NNH<sub>2</sub> interaction, they identified the (CH<sub>3</sub>)<sub>2</sub>NNH product but no mass signal corresponding to the (CH<sub>3</sub>)<sub>2</sub>NN product was seen. And finally in the O + CH<sub>3</sub>-NHNH<sub>2</sub> interaction, the products CH<sub>3</sub>NNH (not CH<sub>3</sub>NHN) and CH<sub>3</sub>NHNH or CH<sub>3</sub>NNH<sub>2</sub> were identified. No actual yields for the carbonaceous species were reported. However, from these product studies they concluded that the predominant simultaneous abstraction of two H atoms in the O + N<sub>2</sub>H<sub>4</sub> → N<sub>2</sub>H<sub>2</sub> + H<sub>2</sub>O reaction most likely occurs by the removal of one hydrogen from each of the nitrogens. It follows that this mode of O atom attack is probably negligible in the O + (CH<sub>3</sub>)<sub>2</sub>NNH<sub>2</sub> reaction but is competitive with the single-H atom removal, O + CH<sub>3</sub>-NHNH<sub>2</sub> → OH + CN<sub>2</sub>H<sub>5</sub>, in the case of methylhydrazine's reaction. Similarly, in another mass spectrometric study by Gerhing and co-workers,<sup>13</sup> a relatively large signal for the primary H<sub>2</sub>O product compared to OH was also observed in the O + N<sub>2</sub>H<sub>4</sub> system.

In this study the temperature dependencies of *k*<sub>1</sub> and *k*<sub>2</sub>, in the range 232–644 K and in 2.0 Torr He pressure, are reported for the first time, and the effect of pressure on *k*<sub>3</sub>(298 K) investigated for He or N<sub>2</sub> buffer gas pressures of up to 404 Torr. We have also measured the OH product yields at 298 K in these reactions and used this information to gain some further insight into the nature of the reaction mechanism in the O + diamine system.

### Experimental Technique

Previously, we have described the details of the fast flow-tube apparatus and the pulsed-photolysis reactor.<sup>14,16</sup> Here, we only give the details of reagent preparations, and how the reaction kinetics data were collected and analyzed.

The diamine plus O atom reactions were studied under pseudo-first-order conditions in O atom concentration ([O atom] ≪ [diamine]). The gas phase [diamine] concentration in the experiments was determined by UV photometric techniques, and accurate measurements of the system's pressure, temperature, and carrier gas flow rates using previously calibrated capacitance manometers, thermocouples and electronic mass-flow meters. The UV-absorption cross sections,  $\sigma_{213.9\text{-nm}}$  of 220.5 × 10<sup>-20</sup>, 248.9 × 10<sup>-20</sup> and 399.9 × 10<sup>-20</sup> cm<sup>2</sup> molecule<sup>-1</sup>, respectively, for N<sub>2</sub>H<sub>4</sub>, CH<sub>3</sub>NHNH<sub>2</sub>, and (CH<sub>3</sub>)<sub>2</sub>NNH<sub>2</sub> were used.<sup>16,17</sup> The Teflon/Pyrex flow-lines were previously conditioned with the diamine so that its in-situ decomposition in the reactors was negligible. For the fast flow-tube apparatus, the O atoms were generated either in a fixed sidearm or in a sliding injector microwave discharge port. A 1% O<sub>2</sub> in He mixture was discharged to produce the O atoms. The inside walls of the port were coated with a 30% solution of H<sub>3</sub>PO<sub>4</sub> acid to minimize O atom loss before being injected into a known amount of the diamine being carried by He with a total linear bulk-flow velocity *v*. The diamine entered the main reaction zone of the flow-tube from the sliding injector when the O atoms were produced upstream in a sidearm, and from the sidearm when the O atoms were made in the sliding injector. The flow-tube was operated under plug-flow conditions<sup>18</sup> at a nominal He

pressure of 2.0 Torr and in the temperature range 232–644 K. A halocarbon coated Pyrex flow-tube with an outer Pyrex jacket that contained a thermostated cooling/heating fluid was used for temperatures below 373 K, and a resistively heated quartz flow-tube (previously cleaned in H<sub>3</sub>PO<sub>4</sub> solution) was used for higher temperature work. Data below 232 K was not obtained as the loss rate of O atoms to the walls in the presence of the diamine was so high that the signal-to-noise ratio of the O atom resonance fluorescence fell below the detection limit of ~5 × 10<sup>8</sup> molecules cm<sup>-3</sup> (signal-to-noise ratio = 1, 1 s integration time). The flow-tube had to be warmed to 232 K or above in order to recover the O atom signal to its original level. Similarly, data above 644 K was not collected as the tendency for charring inside the flow-tube due to alkylated diamine decomposition was observed to increase greatly for *T* ≥ 650 K. At each [diamine], the kinetics of the O atom plus diamine reaction was followed by recording the steady-state O atom cw-resonance fluorescence signal strength as a function of the reaction distance, *z* between the point of reagent mixing at the injector tip and the fixed detection zone downstream of the flow-tube. The O atoms were probed using a cw-microwave atomic resonance lamp to excite the (3<sup>3</sup>S<sub>0</sub> ← 2<sup>3</sup>P<sub>1</sub>) transitions in atomic oxygen. The 130.2–130.6 nm resonance fluorescence ensuing from the detection zone was detected orthogonally to the lamp using a vacuum-monochromator/PMT assembly. The signals were analyzed using photon-counting/multichannel scaling techniques and recorded at a microcomputer for later analysis.<sup>14</sup> The OH product profiles were recorded with sufficient H<sub>2</sub>O added to the flow-tube mixture that it preferentially quenched any OH(*v*' > 0) formed to its ground (*v*' = 0) state before any significant reactive loss took place.<sup>19</sup> The OH was probed using a tunable pulsed-laser operating at ~282.15 nm to excite the Q<sub>12</sub> line of the OH transition (A<sup>2</sup>Σ<sup>+</sup>, *v*' = 1 ← X<sup>2</sup>Π, *v*' = 0). The resulting laser-induced fluorescence due to the transitions (A<sup>2</sup>Σ<sup>+</sup>, *v*' = 1 → X<sup>2</sup>Π, *v*' = 1, bandhead at 312.16 nm) and (A<sup>2</sup>Σ<sup>+</sup>, *v*' = 0 → X<sup>2</sup>Π, *v*' = 0, bandhead at 306.36 nm), ensuing from the detection zone was detected orthogonally to the probe laser beam by a second band-pass-filter/PMT assembly. These signals were analyzed using gated charge-integration/signal averaging techniques and recorded at another microcomputer.<sup>14,20</sup> The detection limit for OH was estimated to be ~1 × 10<sup>9</sup> molecules cm<sup>-3</sup> (signal-to-noise ratio = 1, per 1000-pulse-integrations).

A pulsed-photolysis reactor operating under slow-flow conditions was employed to extend the *k*<sub>3</sub>(298 K) rate coefficient measurements for the O + N<sub>2</sub>H<sub>4</sub> reaction in He or N<sub>2</sub> buffer gas pressures of up to 404 Torr. 248-nm laser photolysis (1–5 mJ/cm<sup>2</sup>/pulse) of ~1.0 × 10<sup>13</sup> molecules cm<sup>-3</sup> of ozone (O<sub>3</sub> + *hν* → O(<sup>1</sup>D) + O<sub>2</sub>, followed by O(<sup>1</sup>D) + N<sub>2</sub> → O(<sup>3</sup>P) + N<sub>2</sub><sup>\*</sup>) was employed to directly follow the kinetics of O(<sup>3</sup>P) in excess N<sub>2</sub>H<sub>4</sub> by recording the cw time-resolved resonance fluorescence O atom signal immediately after the photolysis pulse. The O atom rate coefficient data in N<sub>2</sub> was also obtained indirectly by monitoring OH production in the reaction. Here, 193-nm photolysis of N<sub>2</sub>O was used to produce the O(<sup>3</sup>P) and excess CO<sub>2</sub> was used as the OH(*v*' > 0) product quencher.<sup>19</sup> The kinetics was followed by determining the [OH] time profile immediately after the photolysis by recording the relative OH-fluorescence signal strength as a function of the delay time between the photolysis and probe laser pulses. The slow gas flow rate of the reactor and the laser repetition rate were chosen so as to replenish the reaction mixture in the detection zone after every photolytic pulse.

The absolute OH product yields in these reactions were

determined by measuring the relative detection sensitivity for O atoms and OH radicals in our apparatuses using suitable photolytes for which the values of OH and/or O(<sup>3</sup>P) quantum yields are accurately known. This is described in detail in the next section.

**Materials.** He (>99.9997%) from U.S. Bureau of Mines, N<sub>2</sub> (99.9995%) from Spectra Gases, N<sub>2</sub>O (99.99%) from Matheson Gas Products, and CO<sub>2</sub> (99.99%) from Scott Specialty Gases were used as received. Hydrocarbon-free N<sub>2</sub>H<sub>4</sub> (Viking Grade) from Edwards AFB and (CH<sub>3</sub>)<sub>2</sub>NNH<sub>2</sub> (>99.3%) and CH<sub>3</sub>-NHNH<sub>2</sub> (>99.5%) from Olin Chemicals were subjected to several freeze–thaw purification cycles at a grease-less vacuum line, and the purified distillates dried over BaO or CaH<sub>2</sub>. O<sub>2</sub> (99.991%) from Big Three Industry was used as supplied to make up a 1% in He discharge mixture. O<sub>3</sub> was generated by flowing the O<sub>2</sub> through a commercial ozonator and collected in a trap over silica gel at 195 K. Excess O<sub>2</sub> entrained in the gel was pumped off at 77 K. A 2% O<sub>3</sub> in He calibration mixture was prepared in a darkened 12 L flask. The water was distilled in the laboratory.

## Results

**Direct  $k_1$ ,  $k_2$ , and  $k_3$  Determinations.** Since the [diamine] always is in a great excess over the [O atom] in the flow-tube, it can be shown that the pseudo-first-order decay coefficient  $k'_1$  for O atoms is given by  $\ln\{^{\circ}S/^{\circ}S_0\} = -k'_1 t$ . Where  $^{\circ}S$  is the net (background-subtracted) steady-state O atom cw-resonance fluorescence signal strength recorded at the detection zone for a reaction time of  $t = z/v$ . The flow-tube reaction distance  $z$  is defined to be the length between the tip of the sliding injector where the O atoms enter and the O atom resonance fluorescence detection axis.  $v$  is the bulk linear flow velocity of the He carrier gas.  $^{\circ}S_0$  is the net signal strength that would be observed for  $z = 0$  and corresponds to the initial concentration [O atom]<sub>0</sub> available at the detection zone.  $k'_i = k'_w + k_i[\text{diamine}]$ , where  $k'_w$  is the first-order loss rate term for O atoms to the walls, and  $k_i$  the absolute second-order O atom reaction rate coefficient with the diamine ( $i = 1$  or  $2$  for (CH<sub>3</sub>)<sub>2</sub>NNH<sub>2</sub> and CH<sub>3</sub>NHNH<sub>2</sub>, respectively). Values of  $k'_i$  in the range 100–600 s<sup>-1</sup> were extracted from nonlinear-least-squares fits to the data points of the observed exponential decays of the O atom signal. In the absence of the diamine,  $k'_w$  was typically found to be ~10–20 s<sup>-1</sup> at 298 K. (For O atoms entering upstream via the fixed sidearm port, there is additional loss of O atoms, which increases as the reaction length is decreased due to increasing amount of exposure to the sliding injector walls. In this case it can be shown that  $k'_i = -k'_{w,\text{in}} + k_i[\text{diamine}]$ , where  $k'_{w,\text{in}}$  is the first-order decay coefficient for O atom loss at the injector walls. This lost rate term  $k'_{w,\text{in}}$  was typically found to be ~5 s<sup>-1</sup> at 298 K, see Figure 1, open circles). The values of  $k'_i$  were plotted as a function of [diamine] to extract the corresponding  $k_i$  values by fitting the data to a linear-least-squares routine, see Figure 2. Figure 3 shows the temperature dependencies of  $k_1$  and  $k_2$  in the range 232–664 K and in 2.0 Torr He pressure.

In the O<sub>3</sub>/N<sub>2</sub>/N<sub>2</sub>H<sub>4</sub> pulsed-photolysis experiments, the O atom signal immediately after the initiating laser pulse was also observed to decay exponentially, with the decay coefficient  $k'_3$  given by  $k'_d + k_3[\text{N}_2\text{H}_4]$ . Here,  $k'_d$  represents the sum of first-order loss rate terms of O atoms due to diffusion out of the detection volume, and reaction with O<sub>3</sub> and background impurities.  $k'_d$  was typically measured to be in the range 25–50 s<sup>-1</sup> and  $k_3$  in the range 500–3000 s<sup>-1</sup>. The 298 K values of  $k_3$  determined from second-order plots were;  $(0.56 \pm 0.08) \times 10^{-11}$ ,  $(0.55 \pm 0.08) \times 10^{-11}$  and  $(0.60 \pm 0.09) \times 10^{-11}$  cm<sup>3</sup> molecule<sup>-1</sup> s<sup>-1</sup> in 21.6 Torr He, 208.9 Torr He, and 205.4 Torr

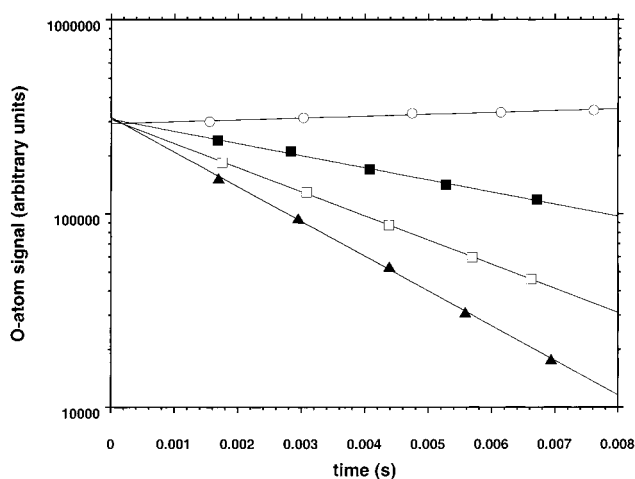


**Figure 1.** Measured O atom resonance fluorescence signal, as a function of flow-tube reaction time,  $t$  in different (CH<sub>3</sub>)<sub>2</sub>NNH<sub>2</sub> concentrations; = zero (open circles), =  $0.587 \times 10^{13}$  (solid squares), =  $0.643 \times 10^{13}$  (open squares), and =  $0.957 \times 10^{13}$  molecules cm<sup>-3</sup> (solid triangles), at 371 K and in 1.96 Torr He. The OH is produced in the sidearm port.

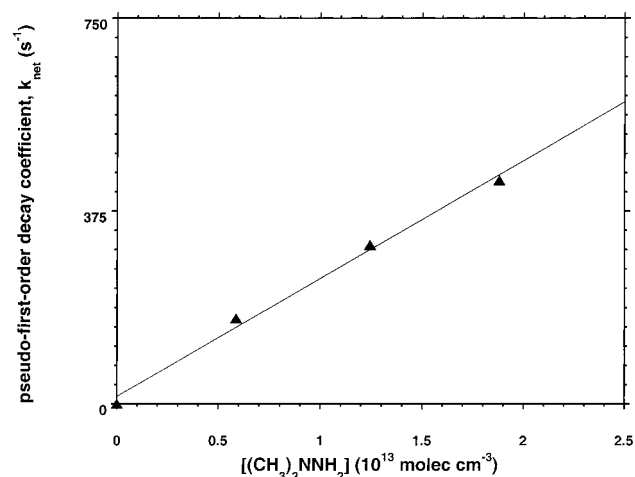


**Figure 2.** Plot of pseudo-first-order decay coefficients,  $k_{\text{net}} = (k'_1 + k'_{w,\text{in}})$  vs the [(CH<sub>3</sub>)<sub>2</sub>NNH<sub>2</sub>] of Figure 1. Because the upward correction, of  $k_{\text{net}}$  for axial diffusion,  $k_{\text{corr}} = k_{\text{net}}(1 + k_{\text{net}}D/v^2)$ , where  $D$ , in units of cm<sup>2</sup> s<sup>-1</sup>, is the diffusion coefficient of O atoms in He is expected to be <5%, ref 18; the flow-tube data was not corrected for this since the other overall errors in the experiment are calculated to be ~±18%, ref 14. The absolute second-order rate coefficient  $k_1$  is determined to be  $(2.05 \pm 0.36) \times 10^{-11}$  cm<sup>3</sup> molecule<sup>-1</sup> s<sup>-1</sup> at 371 K.

N<sub>2</sub> pressure, respectively. All indicated errors in this work are 1 -  $\sigma$ , precision plus estimated systematic.

**OH Product Yield Measurements.** The exothermicity of the O + diamine reaction can produce OH with internal vibrational excitations up to the limit of available reaction enthalpy.<sup>14</sup> To be able to measure accurately the total OH yield in the reaction by just probing the ( $v'' = 0$ ) level, and be able to extract a rate coefficient value for the OH + diamine reaction, it was necessary to record the OH profile in the presence of a suitable quencher that allowed rapid relaxation of OH( $v'' > 0$ ) to the ground state compared to its reactive and/or diffusional loss.

It can be shown that the [OH] profile in the O + diamine flow-tube reaction can be represented by

$$[\text{OH}] = \{(A - B)/(k'_i - k'_{i,\text{OH}})\} \{ \exp(-k'_{i,\text{OH}}t) - \exp(-k'_i t) \} + \{ B/(k'_v - k'_{i,\text{OH}}) \} \{ \exp(-k'_{i,\text{OH}}t) - \exp(-k'_v t) \} \quad (\text{I})$$



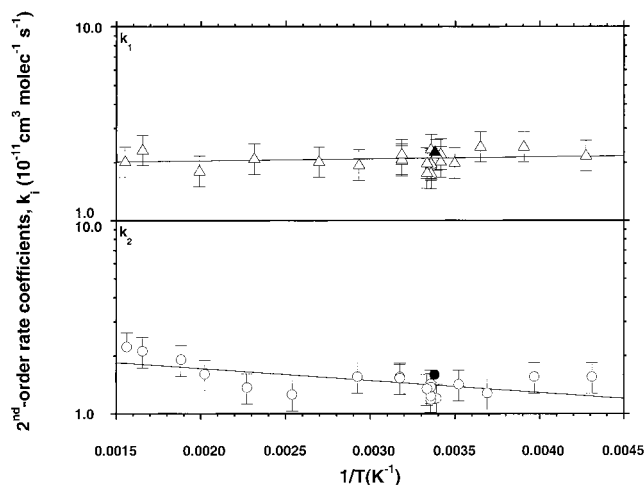
Where  $k'_{i,\text{OH}} = k_{i,\text{OH}}[\text{diamine}] + k'_{\text{w,OH}}$  represents the pseudo-first-order loss of OH in the system, with  $k_{i,\text{OH}}$  as the absolute second-order rate coefficient for OH reaction with the diamine and  $k'_{\text{w,OH}}$  as the first-order rate term for loss to the flow-tube walls.  $k'_\text{v} = k_{i,\text{OH}}^{\text{v}}[\text{diamine}] + k_{\text{OH}}^{\text{v}}[\text{H}_2\text{O}] + k'_{\text{r,OH}} + k'_{\text{w,OH}}^{\text{v}}$  is the effective first-order rate term for decay of vibrationally excited hydroxyl radicals in the system (depicted as OH<sup>v</sup> for all  $v''$  levels), with  $k_{i,\text{OH}}^{\text{v}}$ ,  $k_{\text{OH}}^{\text{v}}$ ,  $k'_{\text{r,OH}}$ , and  $k'_{\text{w,OH}}^{\text{v}}$ , respectively, as the second-order rate coefficient for reaction with the diamine, the second-order rate coefficient for quenching with water, the radiative decay coefficient, and the first-order rate term for loss to the walls. The term coefficients are given by  $A = f_{i,\text{OH}}k_i[\text{O}]_0 - [\text{diamine}]$  and  $B = ((k_{\text{OH}}^{\text{v}}[\text{H}_2\text{O}] + k'_{\text{r,OH}})^{\text{v}}/k_{i,\text{OH}}^{\text{v}}k_i[\text{O}]_0[\text{diamine}]) / (k'_i - k'_\text{v})$ , where  $f_{i,\text{OH}}$  and  $f_{i,\text{OH}}^{\text{v}}$  are the branching fractions for production of OH in ( $v'' = 0$ ) and all excited states, respectively. For our flow-tube conditions during yield measurements of  $4.0 \times 10^{15}$  of H<sub>2</sub>O quencher and  $(0.4\text{--}1.1) \times 10^{13}$  molecules  $\text{cm}^{-3}$  of diamine concentrations, the second term of eq I is negligible, and the expression reduces to  $[\text{OH}] = ((f_{i,\text{OHtot}}k_i[\text{diamine}][\text{O}]_0) / (k'_i - k'_{i,\text{OH}})) \{ \exp(-k'_{i,\text{OH}}t) - \exp(-k'_it) \}$ , where  $f_{i,\text{OHtot}}$  represents the total OH branching fraction in the reaction. The recorded [OH] profiles can thus be fitted, without significant errors, to a three-variable biexponential expression of the form;  $m_1 \{ \exp(-m_2t) - \exp(-m_3t) \}$  to extract values for  $k'_i$  from  $m_3$ ,  $k'_{i,\text{OH}}$  from  $m_2$ , and the total OH yield from  $m_1$ .

Figure 4a shows a typical [OH] profile recorded in the O + CH<sub>3</sub>NHNNH<sub>2</sub> flow-tube reaction. Figure 5a shows values for  $k'_2$  (solid triangles) extracted as a function of [CH<sub>3</sub>NHNNH<sub>2</sub>] employed in the experiment as well as those measured by directly monitoring the O atom decay in the same experiment (open triangles). Figure 5b shows the corresponding plot for  $k'_{2,\text{OH}}$  values. The slopes in these plots give absolute second-order rate coefficient values of  $k_2(298 \text{ K}) = (1.38 \pm 0.34) \times 10^{-11}$  (OH monitoring) and  $(1.43 \pm 0.25) \times 10^{-11}$  (O atom monitoring), and  $k_{2,\text{OH}}(298 \text{ K}) = (5.6 \pm 1.7) \times 10^{-11} \text{ cm}^3 \text{ molecule}^{-1} \text{ s}^{-1}$  in 2.0 Torr He. The corresponding (CH<sub>3</sub>)<sub>2</sub>NNH<sub>2</sub> flow-tube values in 2.0 Torr He were  $k_1(298 \text{ K}) = (2.01 \pm 0.49) \times 10^{-11}$  and  $(2.10 \pm 0.37) \times 10^{-11}$ , and  $k_{1,\text{OH}}(298 \text{ K}) = (6.7 \pm 2.0) \times 10^{-11} \text{ cm}^3 \text{ molecule}^{-1} \text{ s}^{-1}$ .

The photolysis reactor was used to extend the OH yield measurements to higher buffer gas pressures in the O + N<sub>2</sub>H<sub>4</sub> reaction. N<sub>2</sub>O ( $5.0 \times 10^{15}$  molecules  $\text{cm}^{-3}$ ) was photodissociated at 193 nm (1.5 mJ/cm<sup>2</sup>/pulse) in the presence of N<sub>2</sub> to generate the O(<sup>3</sup>P), and the OH profile recorded with sufficient CO<sub>2</sub> ( $8.1 \times 10^{16}$  molecules  $\text{cm}^{-3}$ ) also present to preferentially relax the vibrationally excited OH to its ground state before significant reactive loss occurred. Figure 4b shows a typical OH plot obtained, and the line is a fit to the data points for a kinetic expression analogous to eq I. At each of the 21.2, 185.8, and 404.0 Torr of N<sub>2</sub> pressures studied, the absolute second-order rate coefficient values of  $k_3(298 \text{ K}) = (0.63 \pm 0.16) \times 10^{-11}$ ,  $(0.60 \pm 0.15) \times 10^{-11}$  and  $(0.62 \pm 0.16) \times 10^{-11}$ , and  $k_{3,\text{OH}}(298 \text{ K}) = (3.9 \pm 1.2) \times 10^{-11}$ ,  $(3.8 \pm 1.1) \times 10^{-11}$ , and  $(3.2 \pm 1.0) \times 10^{-11} \text{ cm}^3 \text{ molecule}^{-1} \text{ s}^{-1}$ , respectively, were deduced from the OH profiles. Direct O atom monitoring (to deduce  $k_3$ ) in these experiments was not performed since the N<sub>2</sub>O caused a severe loss in the resonance fluorescence signal due to its huge absorption cross section at  $\sim 130 \text{ nm}$ .<sup>21</sup>

Extraction of the absolute branching fraction for OH production in the O + diamine reactions from fitted values of  $m_1$  (using  $m_2$  and  $m_3$ ) requires instrument calibration using a suitable photolyte. In the flow-tube work, it can be shown that

$$m_1(m_3 - m_2)(R^{\text{O}}/R^{\text{OH}})^{\text{O}}S_0 = (f_{i,\text{OH}} + \sim f_{i,\text{OH}}^{\text{v}})k_i[\text{diamine}] \quad (\text{II})$$



**Figure 3.** Arrhenius temperature dependencies of the absolute second-order rate coefficients;  $k_1$  and  $k_2$  for O atom reactions with (CH<sub>3</sub>)<sub>2</sub>NNH<sub>2</sub> (open triangles) and CH<sub>3</sub>NHNH<sub>2</sub> (open circles), respectively. The 1 -  $\sigma$  error bars represent, on average, an overall uncertainty of  $\sim \pm 18\%$  in the rate coefficient values. Previous room-temperature results for  $k_1$  (solid triangle) and  $k_2$  (solid circle) from ref 11 are also shown.

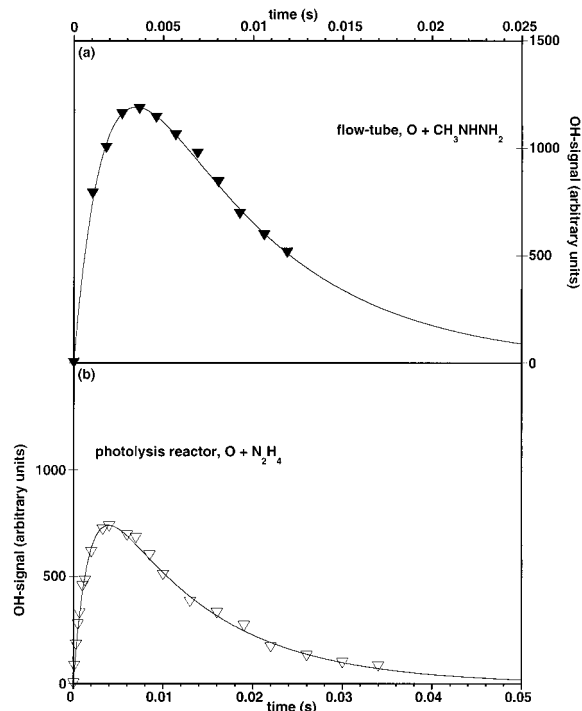


**Figure 4.** (a) OH appearance profile in O + CH<sub>3</sub>NHNNH<sub>2</sub> reaction studied in the flow-tube apparatus. (b) OH appearance profile in O + N<sub>2</sub>H<sub>4</sub> reaction during 193 nm photolysis of N<sub>2</sub>O ( $2.1 \times 10^{15}$ ) in N<sub>2</sub> ( $6.9 \times 10^{17}$ ) and CO<sub>2</sub> ( $8.1 \times 10^{16}$  molecules  $\text{cm}^{-3}$ ). The laser fluence was  $\sim 1.5 \text{ mJ/cm}^2/\text{pulse}$ , and N<sub>2</sub>H<sub>4</sub> concentration was  $1.10 \times 10^{13}$  molecules  $\text{cm}^{-3}$ . The characteristic coefficients of appearance and decay in the signals yield values for  $k'_{i,\text{OH}}$  and  $k'_i$ , respectively. Where  $k'_i$  and  $k'_{i,\text{OH}}$ , are respectively, the first-order rate coefficients for O atom and OH radical reactions in the system.

Where  $^{\text{O}}S_0$  is the O atom signal at  $z = 0$  determined directly from the [O atom] decay recorded in the same experiment as the [OH] profile. ( $R^{\text{O}}/R^{\text{OH}}$ ) is the relative response factor for O atom and OH detection at the two detector assemblies. This is determined in a back-to-back calibration experiment by photodissociating a small amount of O<sub>3</sub> ( $2.0 \times 10^{13}$  molecules  $\text{cm}^{-3}$ ) at 193 nm (1.5 mJ/cm<sup>2</sup>/pulse) in the detection volume of the flow-tube with the same amount of H<sub>2</sub>O ( $4.0 \times 10^{15}$  molecules

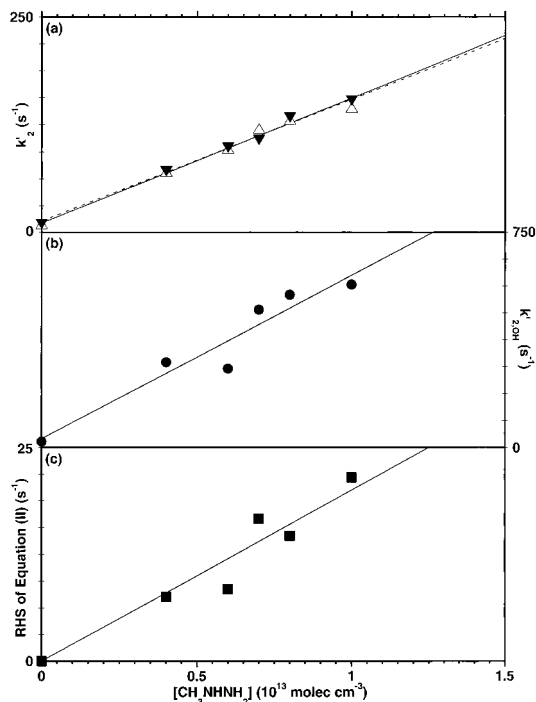


**Figure 5.** Second-order plots for O + CH<sub>3</sub>NHNH<sub>2</sub> flow-tube reaction at 298 K and in 2.0 Torr He pressure: (a) decay coefficients  $k_2$  directly determined by O atom detection (open triangles) and by fitting observed OH product profile of Figure 4a to a biexponential kinetic expression (solid triangles); (b) the corresponding appearance coefficients  $k_{2,\text{OH}}$  in the biexponential fit; (c) phenomenological OH branching coefficient (RHS of eq II) determined by comparison of growth in the OH signal relative to decay of the O atom signal, see text.

$\text{cm}^{-3}$ ) and He (2.0 Torr) present as that employed in the kinetic runs. This ensured that the detection sensitivity for O atoms and OH radicals remained unchanged in the back-to-back runs. The exponential [OH] and [O<sup>3</sup>P] decays are simultaneously recorded in the calibration run, keeping the O atom microwave lamp output and OH-probe laser energy the same as that used in the kinetic run. Care is taken to ensure that the 193 nm photolysis laser beam completely encapsulates the counter propagating light beam from the microwave lamp inside the detection volume. The signals are extrapolated to time zero to determine the value for the ratio of the initial OH and O atom signals,  $(^{\text{OH}}S_{\text{O,cal}}/^{\text{O}}S_{\text{O,cal}}) = (R^{\text{OH}}/R^{\text{O}})([\text{OH}]_{\text{O,cal}}/[\text{O}]_{\text{O,cal}})$ . The ratio  $([\text{OH}]_{\text{O,cal}}/[\text{O}]_{\text{O,cal}})$  for the initial OH and O atom production is directly calculable from the known OH yield in H<sub>2</sub>O photolysis,<sup>22,23</sup> O(<sup>1</sup>D) and O(<sup>3</sup>P) yields in O<sub>3</sub> photolysis,<sup>24</sup> and product yields in O(<sup>1</sup>D) + H<sub>2</sub>O and O(<sup>1</sup>D) + O<sub>3</sub> reactions.<sup>25</sup> Since a large excess of [H<sub>2</sub>O] relative to [diamine] is employed, the weak [diamine] dependence of the  $f_{i,\text{OH}}^{\text{V}}$  term is ignored in the analysis. Also, it can be shown that under these conditions, ~98% of the OH( $v'' > 0$ ) will be quenched to the ground state. Therefore, the value of  $(f_{i,\text{OH}} + \sim f_{i,\text{OH}}^{\text{V}})$  will underestimate the true total OH yield by only ~2% or so. Figure 5c shows a plot of  $m_1(m_3 - m_2)(R^{\text{O}}/R^{\text{OH}})^{\text{O}}S_{\text{O}}$  as a function of  $[\text{CH}_3\text{NHNH}_2]$ , whose slope gives a value for  $(f_{2,\text{OH}} + \sim f_{2,\text{OH}}^{\text{V}})k_2(298 \text{ K}) = (0.20 \pm 0.10) \times 10^{-11} \text{ cm}^3 \text{ molecule}^{-1} \text{ s}^{-1}$  as the phenomenological rate coefficient for the channels that lead to OH formation. Similar analysis for O + (CH<sub>3</sub>)<sub>2</sub>NNH<sub>2</sub> system gave  $(f_{1,\text{OH}} + \sim f_{1,\text{OH}}^{\text{V}})k_1(298 \text{ K}) = (0.24 \pm 0.12) \times 10^{-11} \text{ cm}^3 \text{ molecule}^{-1} \text{ s}^{-1}$ . An estimate for  $f_{i,\text{OH}}^{\text{V}}$  in the flow-tube reactions was made in a different kind of back-to-back experiment. Here, the Q<sub>1</sub>(1) line of the OH(0–0) transition was probed and the resulting fluorescence in the (0→0) band observed in the

presence ( $4.0 \times 10^{15} \text{ molecules cm}^{-3}$ ) and absence of added water at a fixed (~2 ms) reaction time. The signal ratio,  $^{\text{OH}}S_{\text{water}}/^{\text{OH}}S$  is, to a good approximation, directly proportional to  $(f_{i,\text{OH}} + \sim f_{i,\text{OH}}^{\text{V}})/f_{i,\text{OH}}$ , provided  $^{\text{OH}}S_{\text{water}}$  is corrected for the drop in the OH fluorescence quantum yield when water is present in the detection volume. Such analyses at 298 K yielded values of ~53% and ~59% for  $f_{1,\text{OH}}^{\text{V}}$  and  $f_{2,\text{OH}}^{\text{V}}$ , respectively.

Also using the above OH excitation/detection scheme, the phenomenological OH yield in the O + N<sub>2</sub>H<sub>4</sub> reaction was determined by comparing the laser-induced fluorescence signal observed in the 193-nm photolysis of N<sub>2</sub>O/N<sub>2</sub>/CO<sub>2</sub>/N<sub>2</sub>H<sub>4</sub> mixture to that seen in N<sub>2</sub>O/N<sub>2</sub>/CO<sub>2</sub>/H<sub>2</sub>O. It can be shown that

$$m_1(m_3 - m_2)(^{\text{OH}}f_{\text{water}}/^{\text{OH}}f)(D/C)^{\text{OH}}S_{\text{O,water}} = (f_{3,\text{OH}} + \sim f_{3,\text{OH}}^{\text{V}})k_3[\text{N}_2\text{H}_4] \quad (\text{III})$$

Where  $m_i$  ( $i = 1-3$ ), as before, are the best values to a biexponential fit of the [OH] time profile in N<sub>2</sub>O/N<sub>2</sub>/CO<sub>2</sub>/N<sub>2</sub>H<sub>4</sub> photolysis,  $^{\text{OH}}S_{\text{O,water}}$  is the time-zero OH signal in N<sub>2</sub>O/N<sub>2</sub>/CO<sub>2</sub>/H<sub>2</sub>O photolysis, and  $^{\text{OH}}f_{\text{water}}$  and  $^{\text{OH}}f$  represent the OH-fluorescence quantum yield terms in N<sub>2</sub>O/N<sub>2</sub>/CO<sub>2</sub>/H<sub>2</sub>O and N<sub>2</sub>O/N<sub>2</sub>/CO<sub>2</sub>/N<sub>2</sub>H<sub>4</sub> photolysis, respectively.  $D = ([\text{N}_2\text{O}]\sigma_{\text{N}_2\text{O}}Y^{\text{OH}} + [\text{H}_2\text{O}]\sigma_{\text{H}_2\text{O}})$  and  $C = ([\text{N}_2\text{O}]\sigma_{\text{N}_2\text{O}}Y^{\text{O}} + [\text{CO}_2]\sigma_{\text{CO}_2})$ , with  $Y^{\text{OH}} = (1.92[\text{H}_2\text{O}]k_{\text{H}_2\text{O}})/([\text{CO}_2]k_{\text{CO}_2} + [\text{N}_2]k_{\text{N}_2} + [\text{N}_2\text{O}]k_{\text{N}_2\text{O}} + [\text{H}_2\text{O}]k_{\text{H}_2\text{O}})$  and  $Y^{\text{O}} = ([\text{CO}_2]k_{\text{CO}_2} + [\text{N}_2]k_{\text{N}_2} + 0.04[\text{N}_2\text{O}]k_{\text{N}_2\text{O}})/([\text{CO}_2]k_{\text{CO}_2} + [\text{N}_2]k_{\text{N}_2} + [\text{N}_2\text{O}]k_{\text{N}_2\text{O}})$ . The various  $k_{\text{species}}$  are the second-order rate coefficients for O<sup>1</sup>D reactions with the species<sup>25</sup> and the  $\sigma_{\text{species}}$ , the absorption cross sections at 193 nm.<sup>22,25,26</sup> The first term in  $C$  represents the amount of O<sup>1</sup>D from N<sub>2</sub>O photolysis that converts to O<sup>3</sup>P and the second term the amount of O<sup>3</sup>P from direct photolysis of CO<sub>2</sub>. Similarly in  $D$ , the first term represents the amount of O<sup>1</sup>D that converts to OH upon replacing N<sub>2</sub>H<sub>4</sub> with excess H<sub>2</sub>O and the second term the amount of OH from direct photolysis of H<sub>2</sub>O. Calculations of these terms, for our experimental conditions, showed that the contribution to O<sup>3</sup>P from CO<sub>2</sub> photolysis<sup>26,27</sup> was small compared to that from N<sub>2</sub>O,<sup>25</sup> and contribution to OH from H<sub>2</sub>O photolysis<sup>22,23</sup> comparable to that from O<sup>1</sup>D conversion.<sup>25</sup> The ratio,  $(^{\text{OH}}f_{\text{water}}/^{\text{OH}}f) = (k'_{\text{rad}} + [\text{CO}_2]q_{\text{CO}_2} + [\text{N}_2]q_{\text{N}_2} + [\text{N}_2\text{O}]q_{\text{N}_2\text{O}})/(k'_{\text{rad}} + [\text{CO}_2]q_{\text{CO}_2} + [\text{N}_2]q_{\text{N}_2} + [\text{N}_2\text{O}]q_{\text{N}_2\text{O}} + [\text{H}_2\text{O}]q_{\text{H}_2\text{O}})$  is calculable from the known OH( $A, v' = 0$ ) quenching rate coefficients,  $q_{\text{species}}$ <sup>28</sup> and the radiative decay rate  $k'_{\text{rad}}$ ,<sup>29</sup> and the measured species concentrations. This ratio was maintained close to unity (it ranged from 0.989 to 0.927) by using just sufficient amount of water ( $8.0 \times 10^{15} \text{ molecules cm}^{-3}$ ) in the calibration run to convert a small amount (1.5–12.0%) of the O<sup>1</sup>D to OH. The small contribution from N<sub>2</sub>H<sub>4</sub> in  $^{\text{OH}}f$  and  $Y^{\text{O}}$  is ignored in the above analysis. The slopes in the plots of eq III yielded the values  $(f_{3,\text{OH}} + \sim f_{3,\text{OH}}^{\text{V}})k_3(298 \text{ K}) = (0.20 \pm 0.06) \times 10^{-11}$ ,  $(0.24 \pm 0.07) \times 10^{-11}$ , and  $(0.21 \pm 0.06) \times 10^{-11} \text{ cm}^3 \text{ molecule}^{-1} \text{ s}^{-1}$ , respectively, for N<sub>2</sub> pressures of 21.2, 185.8, and 404.0 Torr.

## Discussion

**Reaction Kinetics and OH Yield Measurements.** The reactions of O atoms with the diamines are fast, and show weak temperature dependencies. The Arrhenius fits to the data points of Figure 3 give the following expressions:  $k_1 = (1.94 \pm 0.34) \times 10^{-11} \text{ e}^{(25 \pm 25)/T}$  and  $k_2 = (2.29 \pm 0.40) \times 10^{-11} \text{ e}^{(-145 \pm 40)/T} \text{ cm}^3 \text{ molecule}^{-1} \text{ s}^{-1}$ , respectively, for reactions with (CH<sub>3</sub>)<sub>2</sub>NNH<sub>2</sub> and CH<sub>3</sub>NHNH<sub>2</sub> in the temperature range 232–644 K and in He pressure of 2.0 Torr. Variation in the initial O atom concentration, [O]<sub>0</sub> from  $1 \times 10^{11}$  to  $7 \times 10^{11} \text{ molecules cm}^{-3}$

in the flow-tube had no systematic effect on the  $k_i(298\text{ K})$  values, showing that the influence of any secondary O atom reactions on the rate coefficient determinations is negligible. Previously<sup>14</sup> we had shown that O atoms produced by N<sub>2</sub> microwave discharge followed by N titration with NO gave the same values for  $k_3$  as did the O<sub>2</sub> discharge source. Therefore, O<sub>2</sub>(<sup>1</sup>Δ) from the O<sub>2</sub> discharge is expected to have a negligible effect, if any, on our  $k_1$  and  $k_2$  determinations. The  $k_3(298\text{ K})$  values obtained in the present photolysis reactor are consistent with our earlier values from the flow-tube apparatus. Variation in the 248 nm photolysis fluence (in the range 1–5 mJ/cm<sup>2</sup>/pulse) had no detectable effect on the measured value of  $k'_3$ . Thus, interference from N<sub>2</sub>H<sub>4</sub> photolysis products was also negligible. The O<sub>3</sub> photolyte was added just upstream of the photolysis zone to prevent its excessive loss due to reaction with N<sub>2</sub>H<sub>4</sub>. During the mixture's residence time of ~0.25 s in the reactor, less than 1.7% O<sub>3</sub> loss was estimated to occur for the case when the highest [N<sub>2</sub>H<sub>4</sub>] was employed. The products (OH + O<sub>2</sub> + N<sub>2</sub>H<sub>3</sub>)<sup>30</sup> of this reaction are also expected to cause a negligible interference to our rate measurements. No attempt was made to measure  $k_1$  and  $k_2$  by photolyzing O<sub>3</sub> in (CH<sub>3</sub>)<sub>2</sub>NNH<sub>2</sub> or CH<sub>3</sub>-NHNH<sub>2</sub> (in the presence of N<sub>2</sub>) since these mixtures are expected to be more than 10 times or so less stable than the O<sub>3</sub>/N<sub>2</sub>H<sub>4</sub> mixture.<sup>30</sup>

Also, no discernible pressure effect on  $k_3(298\text{ K})$  was observed for up to 404 Torr of He or N<sub>2</sub>. Our average value for  $k_3(298\text{ K})$  in this work is  $(0.59 \pm 0.12) \times 10^{-11}\text{ cm}^3\text{ molecule}^{-1}\text{ s}^{-1}$ . The present flow-tube  $k_1(296\text{ K})$  and  $k_2(296\text{ K})$  values are in excellent agreement, within ~10% and ~14%, respectively, to those of Lang's determined in a photolysis reactor,<sup>11</sup> though their  $k_3(296\text{ K})$  value is ~68% higher than ours. Assuming that the [diamine] can be measured accurately in these two studies (to within ± ~6% in our work), the presence of reactive impurities in Lang's sample of N<sub>2</sub>H<sub>4</sub> may be a possible cause for the higher measured rate coefficient. The present values of  $k_{1,\text{OH}}(298\text{ K}) = (6.7 \pm 2.0) \times 10^{-11}$ , and  $k_{2,\text{OH}}(298\text{ K}) = (5.6 \pm 1.7) \times 10^{-11}$  in 2.0 Torr He and the average value of  $k_{3,\text{OH}}(298\text{ K}) = (3.6 \pm 1.2) \times 10^{-11}\text{ cm}^3\text{ molecule}^{-1}\text{ s}^{-1}$  in up to 404 Torr He or N<sub>2</sub> pressure are entirely consistent with our direct flow-tube measurements of  $(6.0 \pm 1.1) \times 10^{-11}$ ,  $(6.1 \pm 1.1) \times 10^{-11}$ , and  $(3.7 \pm 0.7) \times 10^{-11}\text{ cm}^3\text{ molecule}^{-1}\text{ s}^{-1}$ , respectively.<sup>31</sup>

The phenomenological branching fraction  $B_{i,\text{OH}}$  for total OH yield in the reactions can be calculated from the ratio of the measured slope(s) of eq II (or III) and the corresponding fitted value of  $k_i$ . These were  $B_{1,\text{OH}} = (0.12 \pm 0.09)$  and  $B_{2,\text{OH}} = (0.14 \pm 0.10)$  at 298 K and in 2.0 Torr He, and  $B_{3,\text{OH}} = (0.32 \pm 0.13)$ ,  $(0.40 \pm 0.15)$ , and  $(0.34 \pm 0.13)$ , respectively, in 21.2, 185.8, and 404 Torr N<sub>2</sub>, and 298 K. Our previous  $B_{3,\text{OH}}$  value determined in the flow-tube work was  $(0.15 \pm 0.05)$  at 298 K and in 2.0 Torr He. In both the flow-tube and photolysis work we consistently measure a low phenomenological yield for OH in the O + N<sub>2</sub>H<sub>4</sub> reaction, though the agreement in the absolute values is not within the combined error limits of the two measurements. The value from the photolysis work is probably more reliable than that from the flow-tube work since much better fits in the OH profiles were possible in this method as data points could be recorded at very short reaction times (~100 μs) and also at very long reaction times where the signal approached to the background level. In the latter flow-tube method, the shortest reaction time used was restricted to ~1 ms to ensure mixing of the reagents downstream of the flow-tube had attained a steady-state condition, and the longest time possible was ~12 ms due to the physical limit of our flow-tube

length. Also from eq III it can be seen that the extracted  $(f_{3,\text{OH}} + \sim f_{3,\text{OH}}^N)k_3$  value relies on only knowing the [N<sub>2</sub>O] and [H<sub>2</sub>O] accurately in the calibration run. These we measured directly using electronic mass flow-meters and 184.9-nm photometry, respectively. Both compounds undergo unit dissociation at 193 nm, via a single photolysis channel, to give (O<sup>1</sup>D + N<sub>2</sub>) and (H + OH) as the products.<sup>23,25</sup> However, in the flow-tube work (eq II), not only must the [H<sub>2</sub>O] and [O<sub>3</sub>] (measured by 253.7-nm photometry) be known correctly, an accurate value is also needed for the ratio of the quantum yield,  $\Phi(\text{O}^3\text{P}):\Phi(\text{O}^1\text{D})$  in the dissociation of ozone, which is known to be a multichannel process at 193 nm. Previously, we have directly determined  $\Phi(\text{O}^1\text{D})$  and  $\Phi(\text{O}^3\text{P})$  to be  $(0.46 \pm 0.29)$  and  $(0.57 \pm 0.14)$ , respectively.<sup>24</sup> Therefore,  $\Phi(\text{O}^3\text{P})/\Phi(\text{O}^1\text{D})$  may be in the range 1.54–0.93. Thus, reanalysis of our earlier work shows that  $(f_{3,\text{OH}} + \sim f_{3,\text{OH}}^N)k_3$  can range from  $1.16 \times 10^{-12}$  to  $0.67 \times 10^{-12}\text{ cm}^3\text{ molecule}^{-1}\text{ s}^{-1}$ . If we include this variability with our flow-tube measurement uncertainties, the nominal value of  $(0.15 \pm 0.11)$  makes the previous phenomenological OH yield in reasonable agreement with the present work. The average value of the two methods is  $(0.30 \pm 0.17)$ . This low phenomenological OH yield in the N<sub>2</sub>H<sub>4</sub> + O atom reaction is qualitatively in agreement with Foner and Hudson's<sup>15</sup> measurements of low signals for the hydrazyl radical (the coproduct of OH) relative to that for the diimide, N<sub>2</sub>H<sub>2</sub>, and Gehring and co-worker's<sup>13</sup> low signals for the OH product relative to that for H<sub>2</sub>O (the coproduct of N<sub>2</sub>H<sub>2</sub>).

The O atom reactions with (CH<sub>3</sub>)<sub>2</sub>NNH<sub>2</sub>, CH<sub>3</sub>NHNH<sub>2</sub>, and N<sub>2</sub>H<sub>4</sub> show significant internal vibrational excitation in the OH product. Our relative measurements provide estimates of ~53%, ~59%, and ~50%,<sup>14</sup> respectively. Production of OH( $v'' = 1$ ) in the alkylated diamine + O atom reactions (in the absence of added H<sub>2</sub>O quencher) was also independently verified in this work by observations of weak LIF signals where the hydroxyl radical was directly excited in the (1←1) band, and the resultant (1→0) and (1→1) band emissions monitored at a monochromator/PMT assembly. No discernible OH LIF signals were seen for (2←2) laser excitation. Thus, most of the vibrationally excited OH is thought to be produced in ( $v'' = 1$ ) state with approximately < 5% of the OH in ( $v'' > 1$ ) levels.

The low OH yields determined in all three O + diamine reactions mean that removal of a single H atom is a minor process at 298 K. Hence direct H abstraction by the O atom from N–H bonds, and when available from C–H bonds, plays a relatively minor role in the overall reaction mechanism. Removal of hydrogen atom(s) could also well occur in an addition–elimination process. The observed negative temperature dependencies of  $k_i$ , for  $T < 500\text{ K}$ , and the lack of pressure effect on  $k_3$  or  $B_{3,\text{OH}}$  in up to 404 Torr of N<sub>2</sub> pressure would be consistent with the formation of an adduct that rapidly dissociates, in principle, through several different product channels. Formation of a cyclic reaction adduct with the O atom bridged between two H atoms could either eliminate H<sub>2</sub>O (plus the azo cofragment) in simultaneous breaking of two N•••H–O bonds, or OH (plus the hydrazyl cofragment) in a sequential breaking of the N–H•••O–H bond followed by the O–H•••N bond. Bridging may take place either across two H atoms at the same nitrogen or between two H atoms, each one of which is situated at the two different nitrogens. Foner and Hudson<sup>15</sup> concluded that this different-N type of bridging is favored in O + CH<sub>3</sub>-NHNH<sub>2</sub> reaction since the mass spectrometric appearance signal of  $m/e = 44$  ion for (cis) CH<sub>3</sub>NNH (and not the diradical, CH<sub>3</sub>-NHN) could be identified with a stable diimide product,<sup>32</sup> while no  $m/e = 58$  ion signal for the (CH<sub>3</sub>)<sub>2</sub>NN product was seen at



all in the case of  $O + (CH_3)_2NNH_2$  reaction. It could well be that  $CH_3NHN$  and  $(CH_3)_2NN$  are also formed via the same-N kind of bridging, but their rapid rearrangement/dissociation prevented them from being detected in their system. For example, highly excited azomethane would be expected to form from  $(CH_3)_2NN$  rearrangement in the  $O + (CH_3)_2NNH_2$  reaction. The reaction exothermicity of  $\sim 102 \text{ kcal mol}^{-1}$  in this channel would be sufficient to dissociate the azomethane into  $2CH_3 + N_2$ . Previously, it is been shown that photoexcited azomethane (at 193 nm) does indeed fragment, after an efficient  $trans \rightarrow cis$  or  $trans \rightarrow gauche$  isomerization, by the rupture of two C–N bonds via a concerted mechanism.<sup>33</sup> It remains an open question whether chemically activated azomethane in its various isomeric forms if produced in the  $O + (CH_3)_2NNH_2$  reaction also dissociates similarly. Thus, direct mass spectrometric detection of the primary product,  $H_2O$  (or the  $CH_3$  and  $N_2$  fragments of the coproduct) would have been more desirable in Foner and Hudson's work to show whether this mode of O atom attack on  $(CH_3)_2NNH_2$  was important or not. Our low OH yield in  $O + (CH_3)_2NNH_2$  reaction would either support this or the possibility that yet another type of addition adduct is involved in these reactions. The observed increase in the room-temperature reaction rate coefficient along the series:  $N_2H_4$ ,  $CH_3NHNH_2$ , and  $(CH_3)_2NNH_2$ , with rate ratios, 1.0:2.3:3.5, shows that increased methylation is facilitating the formation of such adduct(s). This would be consistent if the O atom, acting as an electrophile, attaches preferentially to the substituted N atom, where the relative electron charge density would be expected to increase with increased methylation along the homologous series. Evidence for such a process may be found in the related amine homologous series:  $CH_3NH_2$ ,  $C_2H_5NH_2$ ,  $(CH_3)_2NH$ , and  $(CH_3)_3N$ , where the room-temperature O atom rate coefficient was observed to increase from left to right, and was independent of the argon buffer gas pressure of 13 to 52 Torr employed,<sup>34</sup> showing here also that H-abstraction from N–H is probably not a predominant reaction path. The observed reactivity trend would, however, be consistent with increased importance of H-abstraction from the C–H bond or adduct formation. The negative temperature dependence seen for the very fast  $(CH_3)_3N + O$  reaction suggests a reaction mechanism involving adduct formation. In this case, direct electrophilic attack at the N-center would yield an excited N-oxime adduct. This can either undergo collisional stabilization or fragmentation to products, or in the case of 1° and 2° amine reactions, the initial N-oxime may first rearrange to another excited adduct, a hydroxylamine, which then either collisionally stabilizes or decomposes to final products. To our knowledge, absolute OH or other possible product yield measurements have not been performed for these amine reactions either. Such studies would be very valuable for discerning which reaction path(s) are important in the O atom oxidation of amines. Hence, by analogy, N-oxime type adduct formation in  $O +$  diamine reactions should upon (rearrangement and) N–N bond cleavage also either lead to a hydroxylamine product plus NH, or  $NH_2$  or HNO and their corresponding cofragments. To date, no direct product studies on these species have been carried out. We plan to carryout LIF measurements of these radical fragments soon to ascertain their phenomenological branching fractions.<sup>35</sup> Also, future OH and OD product yield measurements in O atom reactions with N-deuterated hydrazines ( $(CH_3)_2NND_2$  and  $CH_3NDND_2$ ) or with their methyl-deuterated analogues should provide valuable information on the relative importance of removal of the hydrogen from the methyl functionality compared to that from the N-center.

Even though an Arrhenius fit to  $k_1$  and  $k_2$  for the entire temperature range of 232 to 644 K is possible, the data in Figure 3 for  $T > 500 \text{ K}$  clearly shows an onset of upward curvature in the temperature dependence of  $k_i$ . In this regime, either the diamine pyrolytic products are affecting our rate measurements or the importance of another reaction (possibly direct H-abstraction) is increasing. Future higher temperature rate coefficient and OH yield measurements would be of interest for confirming this observation.

**Thermospheric Plume Chemistry.** From our present data, we calculate  $k_2$  to be  $\sim 2 \times 10^{-11} \text{ cm}^3 \text{ molecule}^{-1} \text{ s}^{-1}$  for a typical low earth orbit (LEO) thermospheric temperature of around  $\sim 880 \text{ K}$ . Assumption of a nominal number density of  $\sim 1 \times 10^9 \text{ molecules cm}^{-3}$  for the ambient O atoms results in an oxidation lifetime of  $\sim 50 \text{ s}$  for the  $CH_3NHNH_2$  fuel fragments in the Space Shuttle thruster plume. The oxidation lifetime of the fuel fragments might be much shorter than this for two reasons. First, the thermal rate coefficient at 880 K could be much higher than that extrapolated from Figure 3, and second, the hyperthermal oxygen atoms,  $O^*$ , in the thermosphere could be reacting with the fuel much more vigorously than the thermal atoms which we have measured here to proceed at  $\sim 1/10$ th the gas kinetic rate. Depending on the direction of the thruster velocity ( $\sim 3.5 \text{ km s}^{-1}$ ) relative to the Shuttle's orbital velocity ( $\sim 7.8 \text{ km s}^{-1}$ ), the diamine molecules can encounter  $O^*$  travelling with relative velocities in the range from 4.3 to  $11.3 \text{ km s}^{-1}$ , which corresponds to collision interaction energies in the range 1.1–7.9 eV. These energetic encounters could have higher overall reaction cross sections and proceed via several different modes of attack. Perhaps direct abstraction rather than addition/elimination could be the predominant reaction mechanism in the hyperthermal regime. This would lead to entirely different kinds of product branching patterns/state distributions, and therefore IR and (possibly UV) chemiluminescence, than that observed in the room-temperature bulb experiments which are characterized by Boltzmann energy distributions. Alternatively, high-energy barrier and/or endothermic channels, and pathways that involve complex geometrical rearrangements with electronic excitement could become more accessible. For the latter type, Orient and co-workers,<sup>36</sup> in their crossed-molecular beam apparatus, have seen evidence for the direct formation of electronically excited radical fragments when very fast,  $\sim 20 \text{ eV}$ , in the laboratory frame (LAB),  $O^*$  encounters the diamine molecule. NH(A) emission was seen for all three diamine reactions under *single-collision* conditions, while CH(A) and CN(B) emissions were seen only for the  $CH_3NHNH_2$  reaction. In an earlier work, they had shown that the threshold for NH(A) production was at  $\sim 7.0 \text{ eV}$ , LAB, in the case of the hydrazine reaction.<sup>37</sup> This suggests  $N_2H_4 + O^* \rightarrow NH(A) + NH_2OH$  is the most likely reaction channel for the observed emission since it has a lower thermodynamic threshold of  $\sim 3.53 \text{ eV}$ , in the center-of-mass frame (CM), compared to other possible channels:  $\rightarrow NH(A) + H_2O + NH$  and  $\rightarrow NH(A) + NH_2 + OH$ , which have CM thresholds of  $\sim 5.32$  and  $\sim 6.28 \text{ eV}$ , respectively. The corresponding minimum  $O^*$  beam energy needed would be  $\sim 5.29$ ,  $\sim 7.98$ , and  $\sim 9.41 \text{ eV}$ , LAB, respectively. Their measured threshold suggests a considerable reaction barrier for excited-state product formation. No measured reaction threshold energies are available for the  $O^* +$  alkylated diamine reactions. However, these should have reaction barriers at least equal to their thermodynamic lower limits. Thus, for  $O^* + CH_3NHNH_2$ , the corresponding product channels:  $\rightarrow NH(A) + CH_3NHOH$ ,  $\rightarrow NH(A) + H_2O + CH_3N$ , and  $\rightarrow NH(A) + CH_3NH + OH$  would have CM thresholds of  $\geq 3.41$ ,  $\geq 2.81$ , and  $\geq 6.22$

eV, respectively. For the Space Shuttle plume, this means that the reactions would turn on at relative velocities of  $\sim 7.44$ ,  $\sim 6.76$ , and  $\sim 8.66$  km s $^{-1}$ , respectively. Indeed, the NH(A) plume-radiation intensity is observed to show a strong angular dependence on the Shuttle's orbital velocity vector relative to its thrust vector, with an observed cutoff somewhere between 30° and 90° (zero and 180°, respectively being wake and head-on ram firings). In their numerical simulations, Viereck and co-workers,<sup>10</sup> did not consider direct NH(A) formation from the raw fuel, but rather from similar O\* reactions with its pyrolytic product, CH<sub>2</sub>NH ( $\rightarrow$  NH(A) + H<sub>2</sub>CO or  $\rightarrow$  NH(A) + H<sub>2</sub> + CO) and combustion products, HNC ( $\rightarrow$  NH(A) + CO) and HNCO ( $\rightarrow$  NH(A) + CO<sub>2</sub>). They ruled out the HNC reaction, since in the plume the HCN isomer should be the favored species, and its reaction with O\* is known to produce strong CN(B $\rightarrow$ X) emissions in the laboratory.<sup>38</sup> The plume radiation at 380 nm due to CN(B $\rightarrow$ X) was much weaker than that at 336 nm due to NH(A $\rightarrow$ X), implying a very low absolute [HNC] relative to that of the NH(A) precursor. The HNCO reaction with its thermodynamic threshold of  $\sim 2.02$  eV, CM, would imply an onset for NH(A) emission at relative collision velocity in LEO of  $\sim 5.78$  km s $^{-1}$ , while the higher  $\sim 2.49$  and  $\sim 2.47$  eV, CM, thermodynamic thresholds for the CH<sub>2</sub>NH reactions would imply onset at  $\sim 6.80$  and  $\sim 6.78$  km s $^{-1}$ , respectively. Consequently, the higher angle(s) (between the orbital and thrust vectors) predicted by the latter reactions for the emission onset gave better agreement with the observations, and therefore, HNCO was also ruled out. Note that the O\* + CH<sub>3</sub>NHNH<sub>2</sub> reaction(s), from above, would also have similar high angle onset(s). It is not clear whether or not Viereck and co-workers explicitly were able to rule out this direct path for NH(A) in their *spacecraft/orbiter contamination representation accounting for transiently emitted species* (SOCRATES) simulations,<sup>39</sup> rather they stipulated that a precursor (CH<sub>2</sub>NH) mole fraction of  $\sim 3 \times 10^{-5}$  and inclusion of its O\* reaction in the code gave a reasonable reproduction of many of the observed NH(A) plume-radiation features, including the variation of its intensity with the ram angle. To our knowledge, neither the O\* + CH<sub>2</sub>NH  $\rightarrow$  NH(A) + H<sub>2</sub>CO (or  $\rightarrow$  NH(A) + H<sub>2</sub> + CO) nor the HNC + O\*  $\rightarrow$  NH(A) + CO, or the HNCO + O\*  $\rightarrow$  NH(A) + CO<sub>2</sub> reactions have been studied in the laboratory. Also, the relative CH<sub>2</sub>NH and CH<sub>3</sub>NHNH<sub>2</sub> concentrations in diamine thermospheric plumes have not been directly measured accurately enough<sup>40</sup> to say conclusively what is the dominant source of the NH(A) radiation. The source region of the hypothesized CH<sub>2</sub>NH species could be the exhaust exit plane or in-situ production in the plume. If latter is the case, then since the fuel's pyrolytic lifetime<sup>41</sup> is expected to be as short as  $\sim 1/50$ th of a second in the vicinity of the spacecraft, the choice of CH<sub>2</sub>NH over CH<sub>3</sub>NHNH<sub>2</sub> reaction as the principle NH(A) source would seem to be very logical. However, pyrolysis of the fuel in the plume would initially give CH<sub>3</sub>NH and NH<sub>2</sub> as the main products. Therefore, the relative importance of CH<sub>3</sub>NH disproportionation reaction to yield CH<sub>2</sub>NH plus CH<sub>3</sub>NH<sub>2</sub> compared to its hyperthermal oxidative loss first needs to be understood properly for LEO conditions before the results of SOCRATES or any other numerical simulations can be correctly interpreted in terms of what dominant processes give rise to the measured NH(A) optical environment of the diamine fueled thermospheric plume.

The (far-field) spectrum of the plume from the Space Shuttle's primary RCS (Figure 3 of ref 10) also shows prominent OH(A $\rightarrow$ X) emissions. We are not aware of any detailed analysis for its emission as a function of the spacecraft's altitude or its

ram angle dependence. The following can be said about the possible nature of its source. If the intensity varies with altitude in a manner that is directly proportional to the O atom density profile, then the reaction is with a precursor which itself was not formed by a prior thermospheric O atom oxidative step, since the latter route would give a variation in intensity that would be quadratic in dependence with the O atom density. Either combustion effluent(s), for example, H<sub>2</sub>O,<sup>42</sup> or raw fuel reaction(s) with the O atoms could produce this radiation. The former reaction with a thermodynamic threshold of  $\sim 4.79$  eV, CM, has been hypothesized to be important since H<sub>2</sub>O is the most abundant hydrogenous species in exhaust plumes. Recent OH(A $\rightarrow$ X) emission data<sup>43,44</sup> of the Progress-M Spacecraft have been analyzed, with some success,<sup>44,45</sup> using the H<sub>2</sub>O + O\*  $\rightarrow$  OH(X) + OH(A) source chemistry. However, the energetically less demanding CH<sub>3</sub>NHNH<sub>2</sub> + O\*  $\rightarrow$  OH(A) + CH<sub>3</sub>N<sub>2</sub>H<sub>2</sub> reaction, with a threshold of  $\sim 2.82$  eV, CM, may also be important at  $\geq \sim 6.78$  km s $^{-1}$  LEO collisional velocity in the case of the Space Shuttle. Thus, one should see an angular onset of OH emission very similar in nature to that observed for NH(A). In principle, the mechanism for this hyperthermal reaction might just be ('direct') H-abstraction with electronic excitation in the OH product. The extent to which translational excitation in the reactant couples to higher electronic degrees of freedom in the product, and its reaction mechanism and dynamics are among the least understood molecular processes in the gas phase. However, the related hyperthermal ions, O<sup>+</sup>, are known to react with diamines to produce UV-vis emissions under laboratory conditions.<sup>46,47</sup> The proposed mechanism for the emission involves two steps: an initial charge transfer (possibly a dissociative) process to give the diamine<sup>+</sup> (or a daughter<sup>+</sup>) ion, followed by a dissociative recombination step of the cation(s) with the residual plasma electrons to give electronically excited fragment(s). Such processes in LEO are expected to be of minor importance since the ion density (of which  $\sim 98\%$  is due to O<sup>+</sup>) is typically  $\sim 10^4$  times less than the ambient O\* density. Since Orient and co-workers<sup>36</sup> did not report UV measurements below  $\sim 325$  nm, we plan to search for OH(A $\rightarrow$ X) emissions in  $\geq 5$  eV O\* atom interactions with N<sub>2</sub>H<sub>4</sub> and CH<sub>3</sub>NHNH<sub>2</sub>.<sup>35</sup>

To our knowledge, an ab initio molecular orbital theory computational study on the O + N<sub>2</sub>H<sub>4</sub> reaction has not been performed. It should be interesting to see if an overall energetic profile typical of an addition-elimination mechanism is calculated at thermal energies, and what the predictions are for the transition states and reaction intermediates. Also, of interest would be RRKM/TS-theory predictions for the absolute value for the rate coefficient and the product branching fractions and their temperature and pressure dependencies, and QCT simulations on the derived PES to ascertain the nature of product state distributions as a function of the collision energy.

## Conclusions

For the first time, the O atom rate coefficients for gas-phase reactions with (CH<sub>3</sub>)<sub>2</sub>NNH<sub>2</sub> and CH<sub>3</sub>NHNH<sub>2</sub> have been measured in the range 232–644 K and in He pressure of 2.0 Torr, and are shown to have weak (negative) temperature dependencies as was the case with the O + N<sub>2</sub>H<sub>4</sub> reaction. The lack of any pressure dependence in the latter reaction and the low OH yields measured in all these three reactions suggest a complex reaction mechanism involving the formation of an initial adduct which then rapidly dissociated into a variety of products. Previous studies have shown H<sub>2</sub>O plus the diimide cofragment to be the dominant products in the reaction. Future experimental product(s) state distribution and/or alignment measurements (for



instance, for the OH product<sup>35</sup>) should provide valuable dynamical/mechanistic information about the predominant forces and torques that are exerted as the transient {ON<sub>2</sub>H<sub>4</sub>}<sup>\*</sup> species unfolds into products.

**Acknowledgment.** Funding for this work was provided by the Air Force Office of Scientific Research under Contract F04611-99-C-0025 with the Air Force Research Laboratory, Edwards AFB, CA 93524.

## References and Notes

- (1) Sutton, G. P. *Rocket Propulsion Elements. An Introduction to the Engineering of Rockets*; Wiley: New York, 1992.
- (2) Trinks, H.; Hoffman, R. J. Experimental Investigations of Bipropellant Exhaust Plume Flowfield, Heating, and Contamination and Comparison With CONTAM Computer Model Predictions. In *Spacecraft Contamination: Sources and Preventions*; Roux, J. A., McMay, T. D., Eds.; Progress in Astronautics and Aeronautics, AIAA: New York, 1984; Vol. 91, p 261.
- (3) Viereck, R. A.; Bernstien, L. S.; Mende, S. B.; Murad, E.; Swenson, G. H.; Pike, C. P. *J. Spacecr. Rockets* **1993**, *30*, 724.
- (4) Viereck, R. A.; Murad, E.; Pike, C. P.; Mende, S. B.; Swenson, G. R.; Elgin, J. B.; Bernstein, L. S.; Lucid, S. J. *Geophys. Res.* **1995**, *A100*, 5819.
- (5) Koch, D. G.; Fazio, G. G.; Hoffmann, W.; Melnick, G.; Rieke, G.; Simpson, J.; Witteborn, F.; Young, E. *Adv. Space Res.* **1987**, *7*, 211.
- (6) Dean, D. A.; Huppi, E. R.; Smith, D. R.; Nadile, R. M.; Zhou, D. M. *Geophys. Res. Lett.* **1994**, *21*, 609.
- (7) Zhou, D. K.; Pendleton, W. R. Jr.; Bingham, G. E.; Thompson, D. C.; Raitt, W. J.; Nadile, R. M. *J. Geophys. Res.* **1994**, *A99*, 19585.
- (8) Bernstein, L. S.; Elgin, J. B.; Pike, C. P.; Knecht, D. J.; Murad, E.; Zehnpfennig, T. F.; Galica, G. E.; Stair, A. T. Jr. *J. Geophys. Res.* **1996**, *A101*, 383.
- (9) Broadfoot, A. L.; Anderson, E.; Sherard, P.; Knecht, D. J.; Viereck, R. A.; Pike, C. P.; Murad, E.; Elgin, J. E.; Bernstein, L. S.; Kofsky, I. L.; Rall, D. L. A.; Blaha, J.; Culbertson, F. L. *J. Geophys. Res.* **1992**, *A97*, 19501.
- (10) Viereck, R. A.; Murad, E.; Knecht, D. J.; Pike, C. P. *J. Geophys. Res.* **1996**, *A101*, 5371.
- (11) Lang, V. I. *J. Phys. Chem.* **1992**, *96*, 3047.
- (12) Shane, E. C.; Brennen, W. *J. Chem. Phys.* **1971**, *55*, 1479.
- (13) Gehring, von, M.; Hoyermann, K.; Wagner, H. Gg.; Wolfrum, J. *Ber. Bunsen-Ges. Phys. Chem.* **1969**, *73*, 956. Gehring, M.; Hoyermann, K.; Schacke, H.; Wolfrum, J. *Int. Symp. Combust. Proc.* **1972**, *14*, 99.
- (14) Vaghjiani, G. L. *J. Chem. Phys.* **1996**, *104*, 5479.
- (15) Foner, S. N.; Hudson, R. L. *J. Chem. Phys.* **1968**, *49*, 3724 and **1970**, *53*, 4377.
- (16) Vaghjiani, G. L. *J. Phys. Chem. A* **1997**, *101*, 4167.
- (17) Vaghjiani, G. L. *J. Chem. Phys.* **1993**, *98*, 2123.
- (18) Howard, C. J. *J. Phys. Chem.* **1979**, *83*, 3 and references therein.
- (19) Raiche, G. A.; Jeffries, J. B.; Rensberger, K. J.; Crosley, D. R. *J. Chem. Phys.* **1990**, *92*, 7258. Dodd, J. A.; Lipson, S. T.; Blumberg, W. A. *M. J. Chem. Phys.* **1991**, *95*, 5752.
- (20) Vaghjiani, G. L.; Ravishankara, A. R. *J. Phys. Chem.* **1989**, *93*, 1948.
- (21) Zelikoff, M.; Watanabe, K.; Inn, E. C. Y. *J. Chem. Phys.* **1953**, *21*, 1643.
- (22) Cantrell, C. A.; Zimmer, A.; Tyndall, G. S. *Geophys. Res. Lett.* **1997**, *24*, 2195; *Geophys. Res. Lett.* **1997**, *24*, 2687.
- (23) Barth, C. A.; Suess, H. E. *Z. Phys.* **1960**, *158*, 85, and Stief, L. J.; Payne, W. A.; Klemm, R. B. *J. Chem. Phys.* **1975**, *62*, 4000.
- (24) Turnipseed, A. A.; Vaghjiani, G. L.; Gierczak, T.; Thompson, J. E.; Ravishankara, A. R. *J. Chem. Phys.* **1991**, *95*, 3244.
- (25) DeMore, W. B.; Sander, S. P.; Howard, C. J.; Ravishankara, A. R.; Golden, D. M.; Kolb, C. E.; Hampton, R. F.; Kurylo, M. J.; Molina, M. J. Chemical Kinetics and Photochemical Data for Use in Stratospheric Modeling. Evaluation No. 12, JPL Publication No. 97-4; Jet Propulsion Laboratory: Pasadena, CA, 1997, and references therein.
- (26) Ogawa, M. *J. Chem. Phys.* **1971**, *54*, 2550.
- (27) Inn, E. C. Y.; Heimerl, J. M. *J. Atmos. Sci.* **1971**, *28*, 838. Kosh, M.; Yoshimura, M.; Matsui, H. *Chem. Phys. Lett.* **1991**, *176*, 519.
- (28) Bailey, E. A.; Heard, D. E.; Paul, P. H.; Pilling, M. J. *J. Chem. Soc., Faraday Trans.* **1997**, *93*, 2915. Wysong, I. J.; Jeffries, J. B. Crosley, D. R. *J. Chem. Phys.* **1990**, *92*, 5218. Copeland, R. A.; Crosley, D. R. *J. Chem. Phys.* **1986**, *84*, 3099. Copeland, R. A.; Dyer, M. J.; Crosley, D. R. *J. Chem. Phys.* **1985**, *82*, 4022.
- (29) German, K. R. *J. Chem. Phys.* **1975**, *63*, 6262.
- (30) Tuazon, E. C.; Carter, W. P. L.; Winer, A. M.; Pitts, J. N., Jr. *Environ. Sci. Technol.* **1981**, *15*, 823.
- (31) Vaghjiani, G. L. *Int. J. Chem. Kinet.* **2001**, in press.
- (32) Foner, S. N.; Hudson, R. L. *Adv. Chem. Ser.* **1962**, *36*, 34.
- (33) Gejo, T.; Felder, P.; Huber, J. R. *Chem. Phys.* **1994**, *195*, 423 and references therein.
- (34) Atkinson, R.; Pitts, J. N., Jr. *J. Chem. Phys.* **1978**, *68*, 911.
- (35) Vaghjiani, G. L. Work in progress.
- (36) Orient, O. J.; Chutjian, A.; Murad, E. *J. Chem. Phys.* **1994**, *101*, 8297.
- (37) Orient, O. J.; Chutjian, A.; Martus, K. E.; Murad, E. *J. Chem. Phys.* **1992**, *97*, 4111.
- (38) Orient, O. J.; Chutjian, A.; Martus, K. E.; Murad, E. *Phys. Rev. A* **1993**, *48*, 427.
- (39) Elgin, J.; Bernstein, L. S. The Theory Behind the SOCRATES Code. Report No. PL-TR-92-2207; Geophysics Directorate, Phillips Laboratory, Hanscom AFB: MA, August 1992.
- (40) Wulf, E.; Zahn, von, U. *J. Geophys. Res.* **1986**, *A91*, 3270.
- (41) Eberstein, I. J.; Glassman, I. *Int. Symp. Combust. Proc.* **1965**, *10*, 365.
- (42) Orient, O. J.; Chutjian, A.; Murad, E. *Phys. Rev. Lett.* **1990**, *65*, 2359.
- (43) Karabadzhak, G. F.; Plastinin, Y.; Khmelinin, B.; Teslenko, V.; Shvets, N.; Drakes, J. A.; Swann, D. G.; McGregor, W. K. Presented at the AIAA 36th Aerospace Science Meeting & Exhibition, Reno, NV, January 1998; Paper AIAA-98-0288.
- (44) Drakes, J. A.; Swann, D. G.; Karabadzhak, G. F.; Plastinin, Y. Presented at the AIAA 37th Aerospace Science Meeting & Exhibition, Reno, NV, January 1999; Paper AIAA-99-0975.
- (45) Karabadzhak, G. F.; Plastinin, Y.; Szhenov, E.; Afanasjev, A.; Drakes, J. A.; McGregor, W. K.; Bradley, D.; Teslenko, V.; Shvets, N.; Volkov, O.; Kukushkin, V.; Gimelshein, S.; Levin, D. A. Presented at the AIAA 38<sup>th</sup> Aerospace Science Meeting & Exhibition, Reno, NV, January 2000; Paper AIAA-00-0105.
- (46) Sonnenfroh, D. M.; Caledonia, G. E.; Lurie, J. In *Proceedings of the 19th Exhaust Plume Technology Subcommittee Meeting*; CPIA Publication 568; Johns Hopkins University, Columbia: MD, May 1991; p 347.
- (47) Gardner, J. A.; Dressler, R. A.; Salter, R. H. *J. Phys. Chem.* **1994**, *98*, 11636.